Pulsating turbulence in a marginally unstable stratified shear flow

W. D. Smyth[1],†, H. T. Pham[2], J. N. Moum[1] and S. Sarkar[2]

[1]College of Earth, Ocean and Atmospheric Sciences, Oregon State University,
Corvallis, OR 97330, USA

[2]Department of Mechanical and Aerospace Engineering, University of California,
San Diego, CA 92093, USA

We describe a simple model for turbulence in a marginally unstable, forced, stratified shear flow. The model illustrates the essential physics of marginally unstable turbulence, in particular the tendency of the mean flow to fluctuate about the marginally unstable state. Fluctuations are modelled as an oscillatory interaction between the mean shear and the turbulence. The interaction is made quantitative using empirically established properties of stratified turbulence. The model also suggests a practical way to estimate both the mean kinetic energy of the turbulence and its viscous dissipation rate. Solutions compare favourably with observations of fluctuating 'deep cycle' turbulence in the equatorial oceans.

Key words: air/sea interactions, shear layer turbulence, stratified turbulence

1. Introduction

Stratified shear flows are common in all natural fluid systems. In the oceans and atmosphere, such flows are invariably turbulent, and the prediction of that turbulence is a problem of both theoretical and practical interest. Turbulent stratified shear flows are often in a state of marginal instability (MI), in which turbulence grows and decays repeatedly while the mean flow fluctuates about a stability boundary (Thorpe & Liu 2009; Smyth & Moum 2013; Smyth *et al.* 2013).

While the MI state is readily understood and observed, the nature of the turbulent fluctuations and their interaction with the mean flow remains mysterious. Here, we describe a simple model of fluctuating turbulence in a marginally unstable flow inspired by oceanographic observations. This example serves both to illuminate some fundamental aspects of the MI state and to make a potentially useful prediction of turbulence intensity.

In the equatorial oceans, we often observe turbulence occurring in distinct pulses separated by a period of several hours. In this study we construct a mathematical model of the upper ocean at night and, applying empirically known characteristics of stratified turbulence, derive a closed set of nonlinear, ordinary differential equations

† Email address for correspondence: smythw@oregonstate.edu

whose equilibrium solution is the MI state. Linearizing about this equilibrium, we find an oscillatory solution and compare it with the observed pulses.

To begin, we review the observations and existing theoretical ideas that provide the context for the paper (§ 2). In § 3, we describe the model and its solutions. The results are compared with observations in § 5. In § 6 we summarize the results and discuss both the potential value and the limitations of the model. Appendices describe our observational methods and a generalized model.

2. Marginal instability and the deep cycle of equatorial turbulence

Upper ocean turbulence increases significantly within about a degree latitude of the equator (Crawford 1982). This turbulence has important practical implications for climate because the equator is the primary site for heat uptake by the oceans. Heat may be transferred quickly to the atmosphere or retained in the ocean for many years, depending on the turbulence. Our long-term objective is to understand the processes that drive that turbulence.

In addition to their climatological significance, the upper equatorial oceans provide a unique natural laboratory for the study of stratified, parallel shear flows. Because the Coriolis acceleration vanishes at the equator, trade winds blow steadily to the west, driving a westward surface current (the south equatorial current, hereafter SEC). This sets up a return flow at depth, the equatorial undercurrent (EUC). The SEC tends to spread away from the equator due to the meridional Coriolis gradient, while the eastward EUC converges on the equator and is therefore much stronger. Solar insolation warms the upper few metres while upwelling (due to the diverging surface current and the converging undercurrent) brings cold water from below, setting up a pycnocline. Turbulence acts as a partial brake on the system, preventing runaway acceleration and leading instead to fluctuations about a forced-dissipative equilibrium state.

The classical picture of upper ocean structure is the 'slab' model (e.g. Pollard & Millard 1970). Driven by wind and surface cooling, turbulence is strong in a layer that extends from the surface to a few tens of metres depth. Within that layer, mean water properties (e.g. density, velocity) are uniform, hence the name surface mixed layer (SML), in which density differs by less than 0.01 kg m^{-3} from its surface value. Below the SML is the pycnocline, where turbulence is much weaker and mean water properties vary with depth. While highly simplified, this picture is valid in much of the world ocean, and idealized models based on it have yielded valuable insights into the leading-order physical processes (e.g. Pollard, Rhines & Thompson 1972; Zervakis & Levine 1995; Alford & Whitmont 2007). At the equator, however, upper ocean structure is distinctly different.

Figure 1 represents one week of *in situ* measurements taken in the equatorial Pacific (see appendix A for further details). Figure 1(*a*) shows the zonal velocity profile. The EUC is clearly evident near 100 m depth, whereas the SEC was relatively weak. The pycnocline was located near the core of the EUC (figure 1*b*).

Figure 1(*c*) shows the turbulent kinetic energy dissipation rate ϵ, defined in appendix A. The SML (solid curve) deepened every night, typically to 20–30 m, as turbulence was amplified by surface cooling. The first thing to notice is that turbulence extends far below the base of the SML, in contrast to the slab model described above. Second, note that this deep turbulence varies diurnally. This suggests that, despite the insulating effect of density stratification, the deep turbulence is influenced by the diurnally varying surface forcing. This turbulence regime is called the deep cycle,
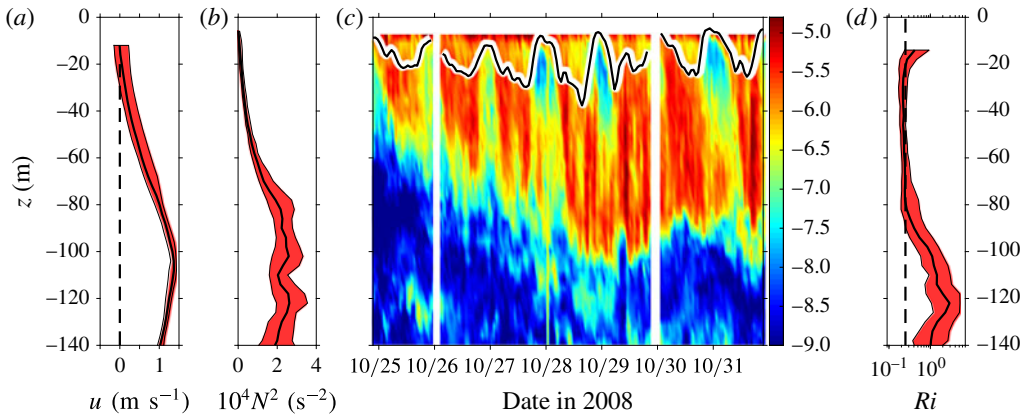
FIGURE 1. Example of deep cycle turbulence in the equatorial Pacific ($0\,^\circ$N, $140\,^\circ$W) over one week in autumn 2008 (Moum *et al.* 2009). (*a*) Zonal velocity *u*. (*b*) Squared buoyancy frequency $N^2 = \partial b/\partial z$, where *b* is the buoyancy. (*c*) Turbulent kinetic energy dissipation rate ϵ as a function of depth and time (UTC). The solid curve represents the base of the surface mixed layer. (*d*) The gradient Richardson number. The dashed curve is the critical value 1/4. In all profiles, the curve is the median and the shaded band represents the quartile range. See Smyth *et al.* (2013) for further details.

and its mechanics have been under study since its discovery in the 1980s (Gregg *et al.* 1985; Moum & Caldwell 1985).

The water below the SML exists in a state of MI, in which the interaction of forcing and turbulent mixing causes the mean flow to fluctuate between stable and unstable states (Thorpe & Liu 2009; Smyth & Moum 2013; Smyth *et al.* 2013). These states can be quantified using the Richardson number *Ri*, the ratio of squared buoyancy frequency ($N^2 = \partial b/\partial z$, where *b* is the mean buoyancy) to squared shear ($S^2 = (\partial u/\partial z)^2 + (\partial v/\partial z)^2$, where *u* and *v* are mean zonal and meridional velocity components and *z* is the vertical coordinate). The flow is stable (unstable) if *Ri* is greater than (less than) a critical value, typically 1/4. In the 2008 observations, *Ri* fluctuated about 1/4 in a layer extending down to 80 m (figure 1*d*).

In our present understanding of the deep cycle, solar heating stabilizes the upper $\sim$10 m, allowing a surface current to build up throughout the day. At sunset, solar stabilization is lost. The surface current then becomes unstable and mixes downwards. Adding to the shear of the EUC, it tips the MI flow into the unstable state, thereby initiating turbulence (Schudlich & Price 1992; Pham, Sarkar & Winters 2013; Smyth *et al.* 2013).

While this scenario explains the diurnal character of the deep cycle, it is not the whole story. On a given night, the deep cycle can involve one or more additional pulses of turbulence. In the example shown in figure 1, these multiple pulses are easily visible in the nights of 26, 27 and 28 October. In previous work, pulses have been identified with internal wave interactions (Moum *et al.* 1992; Peters, Gregg & Sanford 1995) and with shear instability events (Sun, Smyth & Moum 1998). Here, we take a different approach, examining the pulses in the context of the fluctuations expected in marginally unstable turbulence.
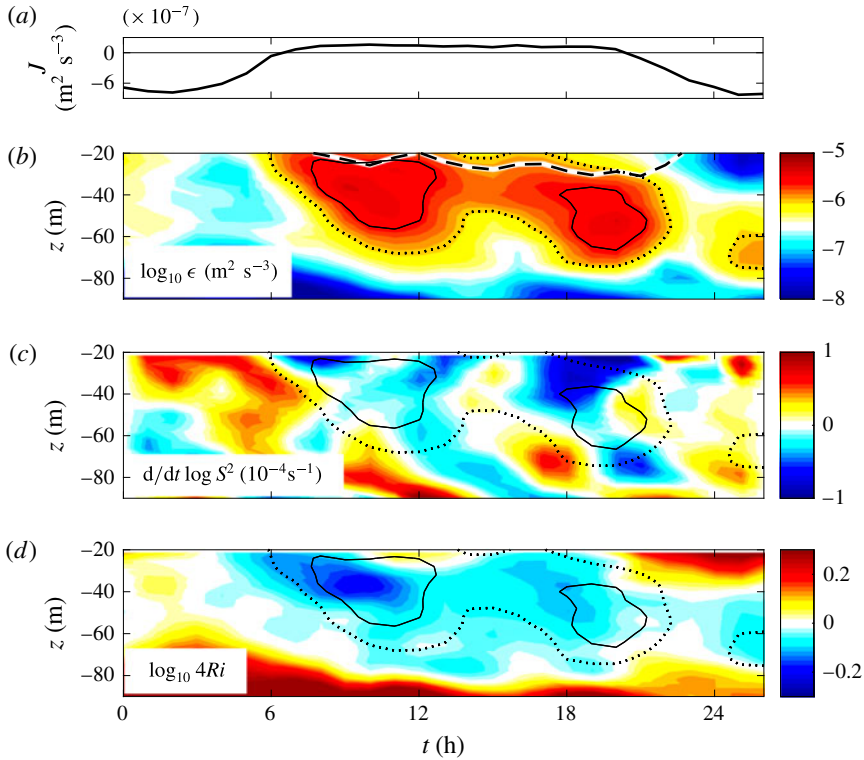
FIGURE 2. A case study of the deep cycle. Measurements are shown for a 26 h period beginning at 10:00 local time, 26 October 2008 (vertical lines on figure 1*c*). Panels show the surface buoyancy flux J (*a*), the turbulent kinetic energy dissipation rate ϵ (*b*), the logarithmic time derivative of S^2 (*c*) and $4Ri$ (*d*). The dashed curve near the top of (*b*) shows the base of the SML. Black contours in (*c*) and (*d*) reproduce the dissipation field from (*b*).

3. A simple model of turbulent pulses

3.1. *A case study*

We hypothesize that the pulses seen in deep cycle turbulence represent a quasi-periodic interaction between turbulence and shear. Consider, for example, the 26 h interval shown in figure 2. The interval begins at 10:00 local time, as solar heating approaches its noon maximum (figure 2*a*). For the first 6 h, turbulence is weak (figure 2*b*), but in late afternoon a turbulent layer appears near the surface and spreads downwards, extending to ∼80 m depth by midnight. This turbulence reaches a maximum, then decays for a few hours. But rather than decay completely, it builds to a second maximum near sunrise ($t \sim 16$–22 h).

This cycle of growing and decaying turbulence is correlated with the growth and decay of shear. The time derivative of squared shear (figure 2*c*) is dominated by descending bands of alternating sign. The first (the yellow–red area at the upper left) precedes the initial turbulence maximum. This corresponds to the augmentation of local shear as the daytime surface current descends (Pham *et al.* 2013; Smyth *et al.* 2013). Subsequently, the shear oscillates, with periods of decay corresponding approximately to periods of strong turbulence.

The cycle is also evident in Ri (figure 2c). During the day, Ri is generally $>1/4$ (yellow–red). Each of the two turbulent events (contours on figure 2c) is preceded by a period in which Ri drops to subcritical values ($<1/4$, blue). In the course of each event, Ri recovers to nearly neutral values (light blue–white–yellow). Depending on how one defines it, the interval between pulses is 8–10 h.

3.2. *Proposed mechanism*

While the example chosen for figure 2 is an especially clear one, inspection of many other cases suggests that the chain of events is common. On this basis, we propose a highly simplified, hypothetical mechanism based on the interaction of shear and turbulence in a stratified fluid forced from above.

Turbulence is forced by shear and dissipated by viscosity, while shear is forced by momentum transport from the wind and is mixed by the downgradient turbulent momentum flux. After sunset, the momentum flux from the descending daytime surface current adds to the existing shear of the EUC, initiating the growth of turbulence. Subsequently the turbulence mixes out the shear. As the turbulence decays, though, the shear is replenished by the momentum flux from above, resulting in another episode of enhanced turbulence.

Is the proposed mechanism consistent with our knowledge of stratified turbulence? To answer this, we extend the classical slab model by adding a second layer below the SML in which deep cycle turbulence exists. Within this layered flow geometry, we use empirically known characteristics of sheared, stratified turbulence to form a closed system of evolution equations. The equations have an oscillatory solution whose characteristics can be compared with the observations.

3.3. *The shear equation*

Space is measured by Cartesian coordinates $\{x, y, z\}$ and flow velocity by $\{u, v, w\}$. The nocturnal SML is modelled as a slab having fixed thickness h, as shown in figure 3. A steady surface stress with friction velocity u_*^2 drives a uniform mean current u. If we take the x direction to be westward, the wind and the current correspond to the trade winds and the SEC. Underlying the SML is a shear layer of fixed thickness H containing the deep cycle, modelled as homogeneous (but non-stationary) turbulence. Beneath this shear layer, the velocity is again uniform and equal to the constant denoted by U.

Assuming that the dynamics is one-dimensional (i.e. no property varies in the horizontal, hence the acceleration is determined solely by the vertical divergence of the momentum flux), we model the acceleration in the SML as

$$\frac{\mathrm{d}u}{\mathrm{d}t} = \frac{u_*^2 + \overline{u'w'}}{h}, \tag{3.1}$$

where $\overline{u'w'} < 0$ is the vertical flux of horizontal velocity at the base of the SML, the overbar represents a horizontal average and primes denote departures from that average. The shear in the deep cycle layer, $S = (u - U)/H$, is governed by the acceleration of the SML:

$$\frac{\mathrm{d}S}{\mathrm{d}t} = \frac{1}{H}\frac{\mathrm{d}u}{\mathrm{d}t} = \frac{u_*^2 + \overline{u'w'}}{Hh}. \tag{3.2}$$
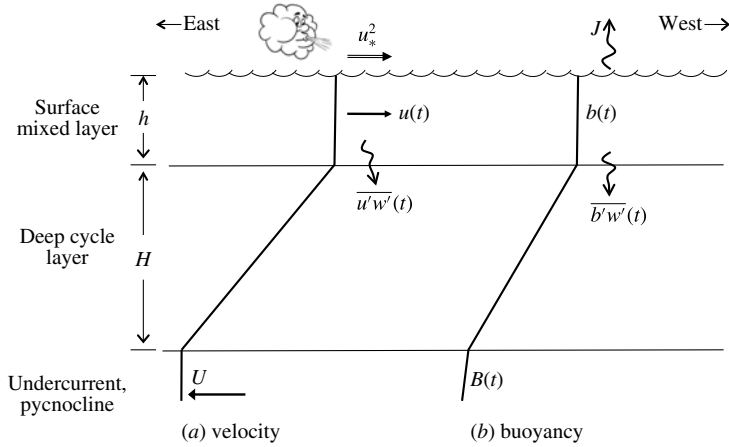
FIGURE 3. Schematic of the upper equatorial ocean, with piecewise-linear profiles of mean velocity (*a*) and buoyancy (*b*).

3.4. *The turbulent kinetic energy equation*

Within the shear layer, the turbulent kinetic energy per unit mass, $k = (\overline{u'u'} + \overline{v'v'} + \overline{w'w'})/2$, is assumed to be spatially homogeneous, and therefore to obey the turbulent kinetic energy equation in the form (e.g. Itsweire *et al.* 1993)

$$\frac{\mathrm{d}k}{\mathrm{d}t} = -\overline{u'w'}S + \overline{b'w'} - \epsilon. \tag{3.3}$$

Terms on the right-hand side are the shear production, the buoyancy production (or vertical buoyancy flux) and the viscous dissipation rate.

3.5. *Closure assumptions*

We now make four assumptions about the turbulence quantities ϵ, $\overline{u'w'}$ and $\overline{b'w'}$ that render (3.2) and (3.3) a closed system.

(i) The ratio of buoyancy flux to dissipation rate, $\Gamma = -\overline{b'w'}/\epsilon$, is called the flux ratio or the mixing efficiency (e.g. Osborn 1980; Moum 1996*a*). While the value of Γ is controversial at present, most estimates agree that it is significantly less than unity. In the ocean turbulence literature, Γ is most often assumed to equal 0.2, while recent results suggest that it is actually smaller than this when turbulence is strong (Ivey, Winters & Koseff 2008). For this reason, we will begin by neglecting $\overline{b'w'}$ in (3.3). Correspondingly, we will approximate the buoyancy gradient N^2 by a constant N_0^2. In appendix B, we relax these assumptions and confirm that the effects of the buoyancy flux are secondary.

(ii) The dissipation rate is modelled as

$$\epsilon = \frac{1}{\tau_N}Nk, \tag{3.4}$$

where $\tau_N = Nk/\epsilon$ is the non-dimensional energy decay time scale. On the basis of ocean microstructure measurements of several hundred turbulent events

with ϵ spanning four decades, Moum (1996*b*) concluded that $\tau_N = 2.1$ with a 95 % confidence limit of ± 0.2. In a survey of laboratory and direct numerical simulation (DNS) studies by Mater & Venayagamoorthy (2014), most estimates lie within a factor 3 to either side of this. Here we choose $\tau_N = 2$ and set $N = N_0$:

$$\epsilon = \tfrac{1}{2} N_0 k. \tag{3.5}$$

(iii) The density-scaled Reynolds stress $\overline{u'w'}$ is related to k by

$$\overline{u'w'} = -2\alpha k. \tag{3.6}$$

The coefficient α is commonly referred to as the Townsend parameter (e.g. Saddoughi 1997). Our assumption here is that α is a known constant. Based on a survey of laboratory experiments, Townsend (1976, p. 108) concluded that, away from boundaries, $\alpha = 0.15 \pm 0.03$ (0.13 near boundaries). Subsequent measurements in a wind tunnel (Saddoughi & Veeravalli 1994; Saddoughi 1997) have confirmed this estimate, as have DNS (e.g. Jacobitz, Sarkar & Van Atta 1997) and *in situ* oceanic observations (Luznik *et al.* 2007).

(iv) With the foregoing three assumptions, equation (3.3) becomes

$$\frac{\mathrm{d}k}{\mathrm{d}t} = \left(2\alpha S - \frac{1}{2} N_0 \right) k. \tag{3.7}$$

The turbulence is in equilibrium ($\mathrm{d}k/\mathrm{d}t = 0$) when

$$\alpha = \frac{1}{4} \frac{N_0}{S}. \tag{3.8}$$

Motivated by observations of marginally unstable turbulence (§ 2), we assume that the equilibrium state is achieved when $Ri_0 = N_0^2/S_0^2 = 1/4$, and therefore that $\alpha = 1/8$. This value is consistent with Townsend (1976) and the other published estimates discussed above.

3.6. *The model equations*

With the closure assumptions listed above, we have a closed pair of evolution equations for the two unknowns $S(t)$ and $k(t)$:

$$\frac{\mathrm{d}S}{\mathrm{d}t} = \frac{1}{Hh} \left(u_*^2 - \frac{1}{4} k \right), \tag{3.9}$$

$$\frac{\mathrm{d}k}{\mathrm{d}t} = \left(\frac{1}{4} S - \frac{1}{2} N_0 \right) k. \tag{3.10}$$

Note the following properties of (3.9) and (3.10).

(i) Because (3.10) is nonlinear, there is no closed-form solution.

(ii) The system preserves the positivity of the kinetic energy, i.e. if $k > 0$ initially, it remains so for all time. To see this, examine (3.10) and note that, as k approaches zero, so does $\mathrm{d}k/\mathrm{d}t$.

(iii) The system has a single equilibrium state, defined by setting the time derivatives to zero:

$$k_0 = 4u_*^2, \quad S_0 = 2N_0. \quad (3.11a,b)$$

The latter statement is equivalent to $Ri = 1/4$, i.e. the equilibrium state corresponds to the state of marginal instability described in §2. Also of interest is the dissipation rate in the equilibrium state, obtained by using (3.11) in (3.5):

$$\epsilon_0 = 2N_0 u_*^2 \quad \text{or} \quad \epsilon_0 = u_*^2 S_0. \quad (3.12a,b)$$

(iv) The character of the solution is oscillatory for all parameter choices. To see this, define S' as the departure of S from its equilibrium value: $S = S_0 + S'$, where S' is not necessarily small. Substituting this into (3.9) and (3.10) and combining gives

$$\frac{d^2 S'}{dt^2} = -\frac{k}{16Hh} S'. \quad (3.13)$$

Provided only that $k > 0$ (see property (ii)), the local curvature of $S'(t)$ has sign opposite to S', signalling an oscillatory solution.

Referring to (3.9) and (3.10), we can qualitatively describe the sequence of events in figure 2 as follows. In early evening, turbulence is relatively weak, hence $k < 4u_*^2$. As a result, dS/dt is positive and shear increases. When shear exceeds $2N_0$ (or, equivalently, $Ri < 1/4$), dk/dt becomes positive and turbulence increases. When k becomes greater than $4u_*^2$, shear decreases, and the cycle repeats.

(v) While (3.9) and (3.10) do not admit a closed-form solution, we can perturb about (3.11) to obtain a quasi-equilibrium solution. In (3.13), we make the substitution $k = k_0 + k'$. We then assume that $|S'| \ll S_0$ and $|k'| \ll k_0$, and linearize accordingly:

$$\frac{d^2 S'}{dt^2} = -\frac{u_*^2}{4Hh} S'. \quad (3.14)$$

The oscillation is now sinusoidal with constant radian frequency given by

$$\omega_0 = \frac{u_*}{2(Hh)^{1/2}}. \quad (3.15)$$

4. Sources of uncertainty

A layer model provides, at best, a crude approximation of the complex structure of the upper ocean. For example, the observational example in figure 2 suggests that the pulsating signal descends in time, a property that could affect the oscillation frequency. To account for this possibility would require a fully depth-dependent model whose complexity would defeat the purpose of the present study.

As in any layer model, there is considerable subjectivity in identifying layer boundaries. We suggest that reasonable estimates of the length scale $(Hh)^{1/2}$ could vary by a few tens of per cent, as the reader may judge by inspection of figures 1 and 2.

Our one-dimensional (vertical) model omits potentially important processes that involve horizontal gradients. These can be approximated by adding new constants to the model. For example, if the wind-driven acceleration of the SML is opposed by a constant horizontal pressure gradient, the result is equivalent to a reduction in the value of u_*, and thus of the pulsation frequency as given in (3.15). If the opposing pressure gradient force is half as strong as the wind stress, the frequency
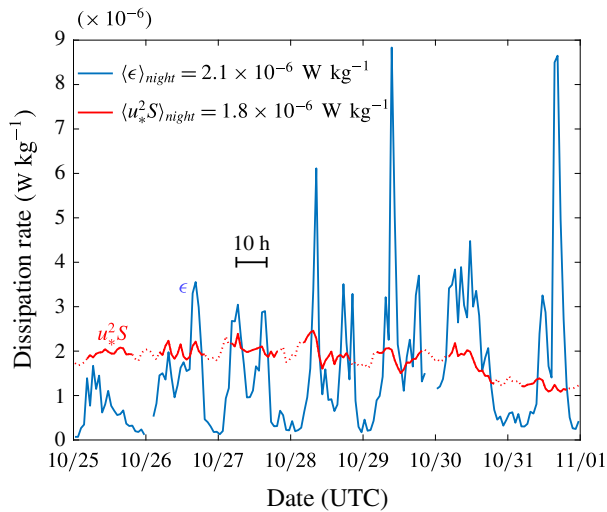
FIGURE 4. Comparison of model predictions with the observations shown in figure 1. Blue curve: observed ϵ (figure 1c) averaged between 20 m and 70 m depth. Red curve: predicted equilibrium value for ϵ, based on (3.12) with root-mean-square shear averaged between 20 m and 70 m depth. Mean values given in the legend are averaged between 19:00 and 10:00 local time, the approximate interval of strong turbulence, also shown by the solid red segments.

is multiplied by $\sqrt{1/2}$, a 30 % reduction. If the pressure gradient reinforces the wind stress, the predicted frequency increases. (Note that the second pulse is expected to happen only if the period is less than about 12 h. Slow variations in the horizontal pressure gradient may therefore explain why the deep cycle exhibits pulses on some nights but not on others.)

A third simplification is the assumption that N is fixed or, equivalently, $\Gamma = 0$. Besides Γ, the turbulence closure involves assuming that three more parameters are constant and have known values, those being α, τ_N and Ri_0. Allowing these parameters to vary dynamically would require a second-order closure model (e.g. Canuto *et al.* 2010), which is beyond our scope here. The assumed constant values, however, are readily altered. In appendix B, we derive a generalized model with time-varying N (i.e. non-zero Γ) that also allows for adjustment of the closure constants. We conclude that the constants are known precisely enough, and Γ is small enough, that these parameters account for only about a 10 % uncertainty in the frequency. The major sources of uncertainty are the layered structure of the model and the neglect of horizontal processes as described above. Based on these uncertainties, we suggest that the generalized model derived in appendix B, while interesting theoretically, is not likely to make more realistic predictions than the simple model described in § 3.

5. Comparison with observations

During the observation period shown in figure 1, winds were steady with mean friction velocity $u_* = 0.011$ m s^{-1}. The dissipation rate ϵ (averaged over 20–70 m; blue curve in figure 4) showed large-amplitude oscillations about a central value near 2×10^{-6} m^2 s^{-3}. Well-defined pulse pairs are visible on 27, 28 and 29 October.

Estimating typical thicknesses for the nocturnal SML and the deep cycle layer, we choose $h = 20$ m and $H = 50$ m. (The former estimated from figure 1; the latter is

based on a typical depth of the contour $\epsilon = 10^{-6}$ W kg^{-1} in figure 2.) With those values, equation (3.15) predicts a period of 10 h. Given the highly simplified nature of both the model and the perturbation solution, this is remarkably consistent with the observations (on figure 4, compare the black bar with typical spacing between peaks).

It is also interesting to compare estimates of the turbulent kinetic energy dissipation rate. The red curve on figure 4 shows this estimate as a function of time, with the solid segments indicating night. (The value used for the shear is the root-mean-square average over the depth range 20–70 m.) On four nights (26–29 October), the observed range of ϵ included the predicted equilibrium value. The nocturnal mean value of ϵ, defined as the average over the hours 19:00–10:00 (local time) when the deep cycle is most active, is 2.1×10^{-6} W kg^{-1}. The predicted equilibrium value $\epsilon_0 = u_*^2 S$, averaged in the same way, is 1.8×10^{-6} W kg^{-1}, smaller by 14 %.

Based on these comparisons, we conclude that the oscillatory shear–turbulence interaction proposed above is plausible as a first-order explanation for the pulsations observed in deep cycle turbulence.

6. Summary and discussion

We have constructed a simple, self-consistent model that incorporates the essential processes responsible for pulsations in marginally unstable stratified turbulence. The model reproduces both the nocturnal mean turbulent dissipation rate and the oscillation period seen in the equatorial deep cycle (e.g. figure 2) to within a few tens of per cent. The model may also be adaptable for other forced, stratified shear flows such as gravity currents and river outflows.

Deep cycle turbulence also exhibits fluctuations more rapid than those described here. For example, close examination of figure 4 shows fluctuations with periods of 4 h or less (e.g. the night of 30 October; also see figure 1c), which the present model does not account for. This suggests that the rapid fluctuations represent a separate phenomenon whose nature remains to be identified.

We are now examining a decade-long record of equatorial turbulence observations in order to more completely characterize pulsations occurring in the deep cycle and compare them with the simplified model described here.

Appendix A. Measurements and data analysis

The observational example shown in figures 1 and 2 is derived from one week of *in situ* measurements taken in the equatorial Pacific at 0°N, 140°W. The mean current velocity (u, v) was measured via a shipboard acoustic Doppler current profiler. Measurements of temperature and conductivity (from which salinity and density were calculated) were made using the free-falling microstructure profiler Chameleon (Moum *et al.* 1995). Chameleon also measured microscale shear down to centimetre scale, from which the turbulent kinetic energy dissipation rate was estimated using the isotropic approximation

$$\epsilon = \frac{15}{4} \nu \left[\left(\frac{\partial u'}{\partial z} \right)^2 + \left(\frac{\partial v'}{\partial z} \right)^2 \right], \tag{A 1}$$

where the partial derivatives represent the vertical shear of two orthogonal horizontal velocity components (e.g. Smyth & Moum 2000).

All data were averaged into bins spanning 1 h in time and 4 m in depth. From these averages, we calculated the squared buoyancy frequency

$$N^2 = -\frac{g}{\rho}\frac{\partial\rho}{\partial z}, \tag{A 2}$$

where g is the gravitational acceleration (9.81 m s^{-2}) and ρ is the density, and the squared shear

$$S^2 = \left(\frac{\partial u}{\partial z}\right)^2 + \left(\frac{\partial v}{\partial z}\right)^2, \tag{A 3}$$

using second-order centred differences. The latter two quantities were combined to form $Ri = N^2/S^2$. Profiles of u, N^2 and Ri shown in figures 1(*a*), 1(*b*) and 1(*d*), respectively, represent the median and the upper and lower quartiles over time in each depth bin.

Wind speed and surface buoyancy flux were measured at a nearby mooring. Wind speed was then converted into the friction velocity u_* using a bulk parametrization (McPhaden 1995).

Appendix B. Generalization of the model

We now generalize the model described in § 3 to allow for time-varying stratification and for adjustments to the turbulence closure parameters. The velocity profile is unchanged; the buoyancy is as shown in figure 3(*b*). The buoyancy of the mixed layer is uniform and is governed by a fixed surface flux J (a good approximation during the night (e.g. Smyth *et al.* 2013)) and a turbulent flux $\overline{b'w'}(t)$ at the mixed layer base:

$$\frac{\mathrm{d}b}{\mathrm{d}t} = \frac{-J + \overline{b'w'}}{h}. \tag{B 1}$$

Note that, at night, both processes have the effect of cooling the SML, i.e. $J > 0$ and $\overline{b'w'} < 0$.

At the base of the deep cycle, the buoyancy is $B(t)$. Within the deep cycle layer, the squared buoyancy frequency is $N^2 = (b - B)/H$, and its time derivative is therefore

$$\frac{\mathrm{d}N^2}{\mathrm{d}t} = \frac{1}{H}\left(\frac{\mathrm{d}b}{\mathrm{d}t} - \frac{\mathrm{d}B}{\mathrm{d}t}\right) = \frac{1}{Hh}(-J + \overline{b'w'}) - \frac{1}{H}\frac{\mathrm{d}B}{\mathrm{d}t}. \tag{B 2}$$

If N^2 is in equilibrium, the lower buoyancy B must decrease (due to equatorial upwelling, perhaps) at a rate equal to the nocturnal cooling of the SML:

$$\frac{\mathrm{d}B}{\mathrm{d}t} = \frac{1}{h}(-J + \overline{b'w'}_0), \tag{B 3}$$

where $\overline{b'w'}_0$ is the equilibrium turbulent buoyancy flux. In view of this, we rewrite (B 2) as

$$\frac{\mathrm{d}N^2}{\mathrm{d}t} = \frac{1}{Hh}(\overline{b'w'} - \overline{b'w'}_0). \tag{B 4}$$

To the closure assumptions listed in § 3.5, we add the assumption that the buoyancy flux and the dissipation rate are related by the fixed coefficient $\Gamma = -\overline{b'w'}/\epsilon$. Combining this with (3.4) gives

$$\overline{b'w'} = -\frac{\Gamma}{\tau_N} Nk, \tag{B 5}$$

and therefore

$$\frac{\mathrm{d}N^2}{\mathrm{d}t} = \frac{1}{Hh}\frac{\Gamma}{\tau_N}(N_0 k_0 - Nk). \tag{B 6}$$

The turbulent kinetic energy equation now includes the buoyancy flux:

$$\frac{\mathrm{d}k}{\mathrm{d}t} = -\overline{u'w'}S + \overline{b'w'} - \epsilon. \tag{B 7}$$

Substituting (3.4) and (B 5) gives

$$\frac{\mathrm{d}k}{\mathrm{d}t} = \left(2\alpha S - \frac{1+\Gamma}{\tau_N}N\right)k. \tag{B 8}$$

The shear equation (3.2), incorporating (3.6), becomes

$$\frac{\mathrm{d}S}{\mathrm{d}t} = \frac{1}{Hh}(u_*^2 - 2\alpha k). \tag{B 9}$$

We next write the three equations (B 9), (B 6) and (B 8) in dimensionless form using the length scale $\sqrt{Hh}$ and the velocity scale u_*:

$$\frac{\mathrm{d}\tilde{S}}{\mathrm{d}\tilde{t}} = 1 - 2\alpha\tilde{k}, \tag{B 10}$$

$$\frac{\mathrm{d}\tilde{N}^2}{\mathrm{d}\tilde{t}} = \frac{\Gamma}{\tau_N}(\tilde{N}_0\tilde{k}_0 - \tilde{N}\tilde{k}), \tag{B 11}$$

$$\frac{\mathrm{d}\tilde{k}}{\mathrm{d}\tilde{t}} = \left(2\alpha\tilde{S} - \frac{1+\Gamma}{\tau_N}\tilde{N}\right)\tilde{k}, \tag{B 12}$$

where tildes indicate non-dimensional quantities. The equilibrium solution is

$$\tilde{k}_0 = \frac{1}{2\alpha}, \quad \frac{\tilde{N}_0}{\tilde{S}_0} = Ri_0^{1/2} = \frac{2\alpha\tau_N}{1+\Gamma}. \tag{B 13a,b}$$

We now make the change of variables

$$\tilde{S} = \tilde{S}_0(1+\sigma), \quad \tilde{N} = \tilde{N}_0(1+\eta), \quad \tilde{k} = \tilde{k}_0(1+\kappa), \tag{B 14a-c}$$

resulting in

$$\frac{\mathrm{d}\sigma}{\mathrm{d}\tilde{t}} = -C_1\kappa, \tag{B 15}$$

$$\frac{\mathrm{d}\eta}{\mathrm{d}\tilde{t}} = -C_2\frac{\eta+\kappa+\eta\kappa}{1+\eta}, \tag{B 16}$$

$$\frac{\mathrm{d}\kappa}{\mathrm{d}\tilde{t}} = C_3(\sigma - \eta)(1 + \kappa),$$ (B 17)

with coefficients C_1, C_2 and C_3 given by

$$C_1 = \frac{\alpha \tau_N}{\tilde{N}_0(1 + \Gamma)}, \quad C_2 = \frac{\Gamma}{2\tilde{N}_0 \alpha \tau_N}, \quad C_3 = \frac{\tilde{N}_0}{\tau_N}(1 + \Gamma).$$ (B 18a−c)

Linearizing about the equilibrium solution $\sigma = \eta = \kappa = 0$ and seeking solutions proportional to $\exp(-\mathrm{i}\tilde{\omega}\tilde{t})$, we are left with a cubic equation for $\tilde{\omega}$:

$$\tilde{\omega}^3 + \mathrm{i}C_2\tilde{\omega}^2 + (C_2 - C_1)C_3\tilde{\omega} - \mathrm{i}C_1 C_2 C_3 = 0.$$ (B 19)

To obtain a simple solution, we treat Γ as a small parameter. In the limiting case $\Gamma = 0$, the non-trivial solution is

$$\tilde{\omega}_0^2 = 2\alpha.$$ (B 20)

If $\alpha = 1/8$, this is equivalent to (3.15). For Γ non-zero but $\ll 1$, we can perturb (B 19) about $\tilde{\omega} = \tilde{\omega}_0$ to obtain:

$$\tilde{\omega} = \tilde{\omega}_0 \left(1 + \frac{\Gamma}{4}\right) + O(\Gamma^2).$$ (B 21)

In dimensional form, this is

$$\omega = (2\alpha)^{1/2} \frac{u_*}{(Hh)^{1/2}} \left(1 - \frac{\Gamma}{4}\right) + O(\Gamma^2).$$ (B 22)

Note that ω is real, i.e. the solution is oscillatory, at least to first order in Γ. With α fixed, replacing $\Gamma = 0$ with $\Gamma = 0.2$ decreases the frequency by 5 %. Using Townsend's (1976) estimate $0.12 < \alpha < 0.18$, we find that the predicted frequency is uncertain by about 5 %. The simplicity of the layer model and the absence of horizontal effects (e.g. pressure gradient) are probably much greater sources of uncertainty than these closure parameters.

The predicted equilibrium dissipation rate ϵ_0 is independent of all closure parameters except Γ:

$$\epsilon_0 = \frac{u_*^2 S_0}{1 + \Gamma},$$ (B 23)

and therefore decreases by about 20 % if Γ is set to 0.2.

REFERENCES

ALFORD, M. H. & WHITMONT, M. 2007 Seasonal and spatial variability of near-inertial kinetic energy from historical moored velocity records. *J. Phys. Oceanogr.* **37**, 2022–2037.

CANUTO, V. M., HOWARD, A. M., CHENG, Y., MULLER, C. J., LEBOISSETIER, A. & JAYNE, S. R. 2010 Ocean turbulence, III: New GISS vertical mixing scheme. *Ocean Model.* **34**, 70–91.

CRAWFORD, W. R. 1982 Pacific equatorial turbulence. *J. Phys. Oceanogr.* **12**, 1137–1149.

GREGG, M. C., PETERS, H., WESSON, J. C., OAKEY, N. S. & SHAY, T. J. 1985 Intensive measurements of turbulence and shear in the equatorial undercurrent. *Nature* **318**, 140–144.

ITSWEIRE, E. C., KOSEFF, J. R., BRIGGS, D. A. & FERZIGER, J. H. 1993 Turbulence in stratified shear flows: implications for interpreting shear-induced mixing in the ocean. *J. Phys. Oceanogr.* **23**, 1508–1522.

IVEY, G. N., WINTERS, K. B. & KOSEFF, J. R. 2008 Density stratification, turbulence, but how much mixing? *Annu. Rev. Fluid Mech.* **40**, 169–184.

JACOBITZ, F. G., SARKAR, S. & VAN ATTA, C. W. 1997 Direct numerical simulations of the turbulence evolution in a uniformly sheared and stratified flow. *J. Fluid Mech.* **342**, 231–261.

LUZNIK, L., ZHU, W., GURKA, R., KATZ, J., NIMMO SMITH, W. A. M. & OSBORN, T. R. 2007 Distribution of energy spectra, Reynolds stresses, turbulence production, and dissipation in a tidally driven bottom boundary layer. *J. Phys. Oceanogr.* **37** (6), 1527–1550.

MATER, B. D. & VENAYAGAMOORTHY, S. K. 2014 A unifying framework for parameterizing stably stratified shear-flow turbulence. *Phys. Fluids* **26** (3), 036601.

MCPHADEN, M. J. 1995 The tropical atmosphere ocean array is completed. *Am. Met. Soc. Bull.* **76**, 739–741.

MOUM, J. N. 1996a Efficiency of mixing in the main thermocline. *J. Geophys. Res.* **101** (C5), 12057–12069.

MOUM, J. N. 1996b Energy-containing scales of turbulence in the ocean thermocline. *J. Geophys. Res.* **101** (C6), 14095–14109.

MOUM, J. N. & CALDWELL, D. R. 1985 Local influences on shear flow turbulence in the equatorial ocean. *Science* **230**, 315–316.

MOUM, J. N., GREGG, M. C., LIEN, R.-C. & CARR, M. E. 1995 Comparison of turbulence kinetic energy dissipation rate estimates from two ocean microstructure profilers. *J. Atmos. Ocean. Technol.* **12** (2), 346–366.

MOUM, J. N., HEBERT, D., PAULSON, C. A. & CALDWELL, D. R. 1992 Turbulence and internal waves at the equator. Part I: Statistics from towed thermistor chains and a microstructure profiler. *J. Phys. Oceanogr.* **22**, 1330–1345.

MOUM, J. N., LIEN, R.-C., PERLIN, A., NASH, J. D., GREGG, M. C. & WILES, P. J. 2009 Sea surface cooling at the equator by subsurface mixing in tropical instability waves. *Nat. Geosci.* **2**, 761–765.

OSBORN, T. R. 1980 Estimates of the local rate of vertical diffusion from dissipation measurements. *J. Phys. Oceanogr.* **10**, 83–89.

PETERS, H., GREGG, M. C. & SANFORD, T. B. 1995 On the parameterization of equatorial turbulence: effect of finescale variations below the range of the diurnal cycle. *J. Geophys. Res.* **100**, 18333–18348.

PHAM, H. T., SARKAR, S. & WINTERS, K. 2013 Large-eddy simulation of deep-cycle turbulence in an upper-equatorial undercurrent model. *J. Phys. Oceanogr.* **43** (11), 2490–2502.

POLLARD, R. T. & MILLARD, R. C. 1970 Comparison between observed and simulated wind-generated inertial oscillations. In *Deep Sea Research and Oceanographic Abstracts*, vol. 17, pp. 813–816, IN5, 817–821. Elsevier.

POLLARD, R. T., RHINES, P. B. & THOMPSON, R. O. R. Y. 1972 The deepening of the wind-mixed layer. *Geophys. Fluid Dyn.* **4** (1), 381–404.

SADDOUGHI, S. G. 1997 Local isotropy in complex turbulent boundary layers at high Reynolds number. *J. Fluid Mech.* **348**, 201–245.

SADDOUGHI, S. G. & VEERAVALLI, S. V. 1994 Local isotropy in turbulent boundary layers at high Reynolds number. *J. Fluid Mech.* **268**, 333–372.

SCHUDLICH, R. & PRICE, J. 1992 Diurnal cycles of current, temperature, and turbulent dissipation in a model of the equatorial upper ocean. *J. Geophys. Res.* **97**, 5409–5422.

SMYTH, W. D. & MOUM, J. N. 2000 Anisotropy of turbulence in stably stratified mixing layers. *Phys. Fluids* **12**, 1343–1362.

SMYTH, W. D. & MOUM, J. N. 2013 Seasonal cycles of marginal instability and deep cycle turbulence in the eastern equatorial Pacific ocean. *Geophys. Res. Lett.* **40**, 6181–6185.

SMYTH, W. D., MOUM, J. N., LI, L. & THORPE, S. A. 2013 Diurnal shear instability, the descent of the surface shear layer, and the deep cycle of equatorial turbulence. *J. Phys. Oceanogr.* **43**, 2432–2455.

SUN, C., SMYTH, W. D. & MOUM, J. N. 1998 Dynamic instability of stratified shear flow in the upper equatorial Pacific. *J. Geophys. Res.* **103**, 10323–10337.

THORPE, S. A. & LIU, Z. 2009 Marginal instability? *J. Phys. Oceanogr.* **39**, 2373–2381.

TOWNSEND, A. A. 1976 *The Structure of Turbulent Shear Flow*. Cambridge University Press.

ZERVAKIS, V. & LEVINE, M. D. 1995 Near-inertial energy propagation from the mixed layer: theoretical considerations. *J. Phys. Oceanogr.* **25** (11), 2872–2889.